

# Removal of Crystal Violet and Acid Red 1 Dyes from Wastewater by Mechanically Activated Talc

Sofia Afifi<sup>1</sup>, Mohsen Farahat<sup>2,\*</sup>, M. A. Abdel Khalek<sup>2</sup>, Farida M. S. E. El-Dars<sup>3</sup>

<sup>1</sup> Rod El Farag Water Treatment Plant, Utility Water Authority for Greater Cairo, Egypt

<sup>2</sup> Central Metallurgical Research and Development Institute (CMRDI), P.O. Box 87, Helwan, Cairo, Egypt

<sup>3</sup> Chemistry Department, Faculty of Science, Helwan University, Ain Helwan, Cairo 11795 Egypt.

\*Corresponding author: E-mail: [mohsen105@hotmail.com](mailto:mohsen105@hotmail.com)

Received 21 October 2023

Accepted 9 December 2023

Published 31 December 2023

## Abstract

Raw talc (RT) and mechanically activated talc (MAT) were prepared and utilized as adsorbents for removing Crystal Violet (CV) and Acid Red 1 (AR1) from aqueous solutions. We investigated the impact of pH, dye concentration, conditioning time, and temperature on the removal efficiency of acid and basic dyes by RT and MAT samples. The results demonstrate that MAT exhibited significantly higher adsorption capacities, with values of 160 mg/g for CV and 130 mg/g for AR1—2-3 times greater than those of RT. Experimental data revealed that the adsorption of both dyes by RT followed the Temkin isotherm, while MAT followed the Freundlich isotherm. Additionally, the adsorption behavior of CV and AR1 on MAT and RT followed a pseudo-second-order process, with intra-particle diffusion being the rate-limiting step for the adsorption kinetics of AR1 onto RT. The enhanced adsorption performance of MAT was attributed to its high pore volume and the presence of multi-charged sites resulting from the rupture of chemical bonds through intensive material grinding. Physical properties of RT and MAT were further investigated using XRD analysis, FTIR, zeta potential, particle size, and Brunauer–Emmet–Teller (BET) analysis. The results revealed that intensive grinding caused significant crystal dislocations in raw talc, leading to a noticeable shift in its isoelectric point (IEP), an increase in surface area, and a decrease in pore size. These findings provide supporting evidence for the observed adsorption results.

**Keywords:** Talc, Mechanical activation, Adsorption, Crystal Violet, Acid Red 1, Wastewater treatment

## 1. Introduction

There are numerous thousands of types of dyes and pigments produced worldwide which amount to approximately 700000 tons [1]. The textile sector consumes a high volume of water as well as chemicals compared to other industries [2]. It was estimated that the average textile industry consumes about 200 liters of potable water per kilogram of product. Due to the variety of processes undertaken within this sector, wastewater discharged from this industry was reported to contain toxic pollutants, including dyes, NaOH, starch, acid, toxic elements, etc. [1,2]. The World Bank estimated that the dyeing and finishing activities of this sector produce near to 17–20% of the total industrial wastewater generated by the industry [2]. The recycling and reuse of these pollutants are viable for saving and

providing additional water resources and minimizing hazardous pollutants discharge into the environment [3]. Around 20 % of this volume is dumped without any prior processing. Thus, concern is building as they may contain loads of heavy metals, nitrates, surfactants, enzymes, VAT dyes, synthetic dyes, and acetic acid that have a detrimental effect on all life forms [1,4].

The synthetic cationic dye (CV), (C<sub>25</sub>H<sub>30</sub>ClN<sub>3</sub>) or methyl violet 10B, is extensively utilized in the textile sector to color silk, cotton, and nylon as well as in inks of printing and biological stains, which are utilized as dermatological agents in veterinary medicine [4-7]. CV is poisonous, can irritate the skin when absorbed through it, and is hazardous when inhaled or consumed. Extreme cases can result in malignancy, severe eye

irritation that can cause blindness for life as well as and kidney failure in addition to being carcinogenic [8,9]. AR1 ( $C_{18}H_{13}N_3Na_2O_8S_2$ ) is a common anionic azo dye that dissolves in water, groups of sulfonic acid exist in the dye structure, in an aqueous solution, giving it a negative charge [10]. AR1 is fundamentally used in wool dyeing through a strong acid medium and can be simply applied to fabrics of wool and fiber of polyamide. AR1 has been used as a food additive, however, studies have shown that Red Acid 1 is altered to poisonous materials, which may eventually interfere with blood hemoglobin as well as being non-biodegradable [11].

Industries have utilized a variety of physicochemical, chemical, and biological treatments over the years to remove colorants, including flocculation, chemical precipitation, adsorption, membrane, electrochemical processes, ozonation, and bio-decolorization [4, 12,13]. Adsorption is considered one of the most efficient modern wastewater treatment methods to minimize dangerous chemicals found in effluents. Due to its low initial cost, easy operation, and superiority over other techniques for removing colors from water, this method is widely used [13,14].

Recently, various mineral particles have been used for dye removal through adsorption. Sepiolite has been employed in particular because it exhibits a higher capacity than traditional adsorbents to remove cationic dyes. This is because sepiolite contains silanol groups (-SiOH) on its external surface, which are available to organic substances as neutral adsorption sites. Additionally, its enormous micropore volume and high specific surface area contributed to its potent adsorbent capabilities. However, the use of sepiolite as an adsorbent is limited in some parts of the world due to its high cost and limited deposit availability. Therefore, to reduce the expenses, researchers have explored alternative minerals that are more affordable and readily accessible. Considering phyllosilicate minerals, talc is a potential substitute due to its resemblance to sepiolite in structure. The primary contrast between these minerals lies in the interruptions and alterations of the silica sheets found in the sepiolite structure, resulting in the formation of structural channels and blocks [15].

Talc is a hydrous magnesium phyllosilicate with a chemical formula ( $Mg_3 [Si_4O_{10}] (OH)_2$ ). The spatial arrangement of "tot" is portrayed by two tetrahedral sheets (t) that are interconnected by Van Der Waals bonds (Fig. 1). These sheets are made up of silicon and oxygen atoms, and they encircle an octahedral sheet (o), which is made up of magnesium and hydroxyl (brucite

leaf). Talc has two forms - monoclinic and triclinic, with monoclinic being the more prevalent. In its crystalline structure of raw talc (shown in Fig.1), there is a triple layer consisting of a magnesium hydroxide sheet and two sheets made up of tetrahedrons of ( $SiO_4^{4-}$ ). The outer siliceous surfaces are polar and oleophilic, hydrophobic, aerophilic, and inert [16]. Because talc possesses unique porosity and high specific surface area, it has a high flexibility for application in adsorption processes [17] in industrial wastewater treatment [18] and for dye removal [19].

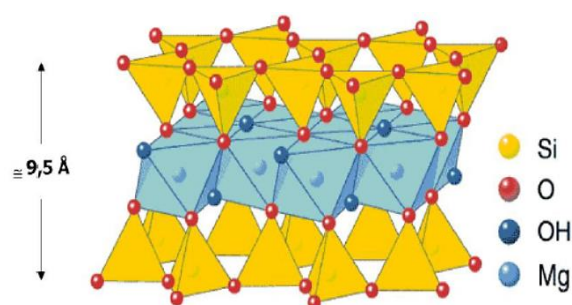


**Fig. 1** Crystal structural of Raw Talc [16].

One approach to improve upon the adsorptive properties of minerals has been mechanical activation of the starting material [20]. Milling reduces the particle size, which increases the surface contact area of the mineral [21,22]. The mechanical activation was reported to lower the mineral temperature, which increases the system's internal energy. This amorphization increases the surface activity and increases the talc reactivity [23-25].

The current research seeks to evaluate and compare the effectiveness of RT and MAT in the removal of CV and (AR1) from aqueous solution. The influence of mechanical activation on the crystallinity and surface properties of talc will also be investigated. The adsorption behavior of the studied dyes onto the mechanically activated and raw talc will be studied to determine optimal conditions for pH, initial dye concentration, adsorbent dose, contact time, and temperature. Thermodynamics and kinetics of the process will be explained and elucidated.

## 2. Experimental

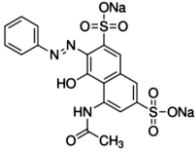

### 2.1. Materials

AR1: an anionic acid dye and CV, a basic synthetic dye (Basic Violet-3) (analytical grade; 99.9% purity (Sigma-Aldrich) and 99.9% purity (Merck), respectively) were used for the preparation of dyes stock solutions with no further purification. Their chemical properties are provided in Table 1. Stock

solutions of acid red 1 and crystal violet (1000 ppm) were prepared. Then, working standard solutions of concentrations (20, 40, 60, 100, 200, and 400 ppm) were prepared. 0.1 M HCl and/or 0.1 M NaOH were used to modify the pH of the solution.

A high-purity talc sample was received as lumps from Wadi El Allaqi deposits in the Eastern Desert, Egypt. The chemical analysis of talc is shown in Table 2.

**Table 1.** General characteristics of Acid red 1 and Crystal Violet dyes.

Character	Acid Red 1 (AR1)	Crystal violet (CV)
Type	Anionic	Cationic
Chemical composition	C <sub>18</sub> H <sub>13</sub> N <sub>3</sub> Na <sub>2</sub> O <sub>8</sub> S <sub>2</sub>	C <sub>25</sub> H <sub>30</sub> ClN <sub>3</sub>
Chemical structure		
Charge	2 <sup>-</sup>	1 <sup>+</sup>
Mol. Wt.	493	407
λ <sub>max</sub> (nm)	506	590
pKa	6.4 [26]	8.64 [27]

**Table 2.** Chemical Composition of Wadi El Allaqi raw talc.

Constitute	SiO <sub>2</sub>	Fe <sub>2</sub> O <sub>3</sub>	MnO	MgO	CaO	Cl	SO <sub>3</sub>	L.O.I	Other
Wt. %	61.4	0.24	0.02	32.8	0.2	<0.01	<0.01	4.7	0.62

## 2.2. Methods

### 2.2.1 Mechanically activated talc

The talc sample was first crushed using Denver-style jaw and roller crushers. The crushed sample was ground in a tumbling mill (ball mill) to get a sample of 100% less than 75 microns (mechanical activation feed). Mechanical activation was further carried out using a planetary ball mill (PULVERISETTE 5 (FRITSCH-Germany)) in a 300 mL stainless steel bowl filled at 50 % for 180 min, at 300 rpm and 15:1 (Ball: powder) with 11 mm diameter stainless steel balls.

### 2.2.2.Characterization

RT and MAT were characterized using XRD-(D8ADVANC) (Bruker Corporation (German)) with LYNXEYE XE-T detector with (λ = 1.54 Å) at 40 kV and 40 mA and 2θ-angles from 3 to 70 ° and energy-dispersive X-ray fluorescence. FTIR analysis was performed using JASCO Spectrometer 6300 (Japan) in the range 400–4000 cm<sup>-1</sup>. Particle size distribution measurement in both samples was analyzed by a laser particle analyzer (BT-2001). Zeta potentials were measured by Zetasizer (Malvern Instrument Co. Ltd., United Kingdom), and BELSORP-MR 6 was used to measure surface area and porosity.

### 2.2.3. Adsorption experiments

The experiments were conducted in 50 mL round bottom flasks where 0.05 g of talc sample was agitated with 25 mL of dye solutions (20-400 mg/L) at different pH (2-12), temperatures (20 – 60 °C), and at various contact time (0-240 min.) using a mechanical shaker-type WISD at 250 rpm. The adsorbent was collected by centrifugation using the SIGMA 2-16P centrifuge. The absorbance of the initial and final AR1 and CV content was measured at λ<sub>max</sub> 506 and 590 nm, respectively, using a UV-visible spectrophotometer (PGInstrumentsT60).

The adsorption capacity (mg.g<sup>-1</sup>) was determined by equation (1):

$$q = \frac{V(C_i - C_f)}{M} \quad (1)$$

While the adsorption efficiency (Removal %) was determined by equation (2):

$$R \% = \frac{C_i - C_f}{C_i} \times 100 \% \quad (2)$$

where  $q$  is the adsorbed amount of dye per gram of adsorbent,  $C_i$  and  $C_f$  are the initial and final dye concentrations, respectively (mg.L<sup>-1</sup>);  $V$  is the volume of the dye solution (L) and  $M$  is the amount of the adsorbent used (g).

## 3. Results and discussion

### 3.1. Material characterization

Figure 2 shows the XRD patterns for RT and MAT samples. The presence of the basal diffraction peaks of raw talc at (002), (004), (006), (132), and (0010) were observed at 2θ angles of 9.48°, 19.02°, 28.64°, 36.26° and 48.72°, respectively, for RT [28-30]. For (MAT), the broadening of the spectrum and the disappearance

of almost all diffraction peaks was evident indicating the significant impact of high milling energy upon the crystal structure of raw talc. This high degree of amorphization of MAT was reported to contribute to its high surface activity [31, 32].

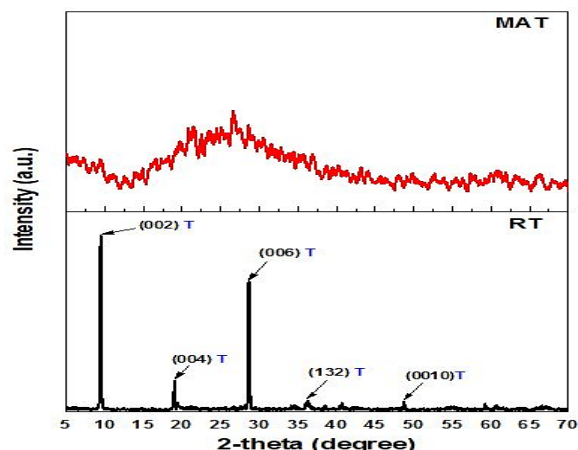


Fig. 2 XRD patterns for RT and MAT

### 3.2. Particle size distribution analysis

Figures 3 and 4 display the particle size distribution and size discrete analysis for both RT and MAT, respectively. The data indicate that the distribution of d90 and d50 for RT was mono-modal at 31.2  $\mu\text{m}$  and 9.09  $\mu\text{m}$ , respectively. For MAT, the d90 and d50 sizes distribution were 27.6  $\mu\text{m}$  and 6.48  $\mu\text{m}$ , indicating a bimodal symmetrical distribution. This may be attributed to the severe grinding conditions that contributed to the breakdown of the raw talc rigid crystal structure.

### 3.3. FTIR analysis

FTIR spectrum for both RT and MAT is shown in Fig. 5 a and b. For RT, the stretching vibrational band of the siloxane group (Si-O-Si) was observed with an intense peak at 460.14  $\text{cm}^{-1}$  and the band at 667.15  $\text{cm}^{-1}$  reflecting the Si-O-Mg bond. The band at 3674.44  $\text{cm}^{-1}$  represents the stretching of the Mg-O/Mg-OH octahedral layer and the band at 1007.56  $\text{cm}^{-1}$  corresponds to the Si-O tetrahedral layer [28,33,34]. It was noticed that for MAT the peaks at 3674.44  $\text{cm}^{-1}$  and 460.14  $\text{cm}^{-1}$  due to the stretching vibration of Mg-O/O-H have disappeared revealing the destruction of (Mg-OH) and (Si-O-Si) bonds due to force milling. As well, the stretching vibration of Si-O-Mg bonds at 1007.56  $\text{cm}^{-1}$  and Si-O at 667.56  $\text{cm}^{-1}$  decreased indicating the impact of mechanical activation upon the talc functional groups [35, 36].

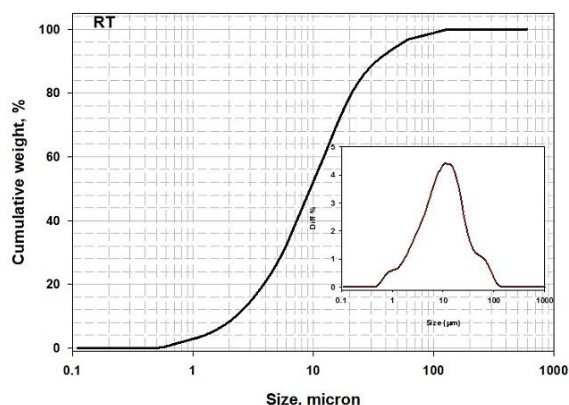


Fig. 3 Particle size distribution analysis for RT.

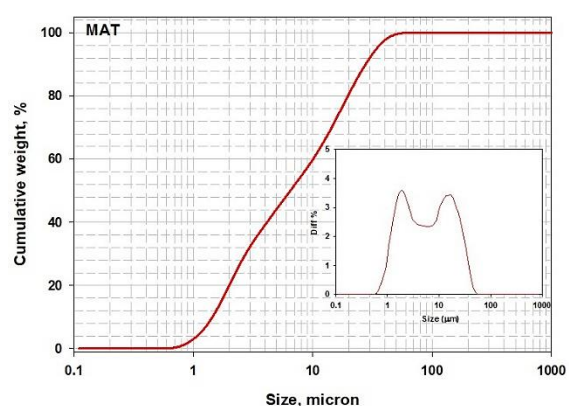


Fig. 4 Particle size distribution analysis for MAT.

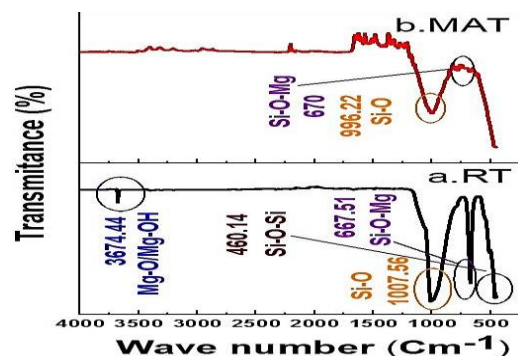


Fig. 5 FTIR spectrum of RT and MAT.

### 3.4. Zeta potential

Figure 6 shows the surface charge of talc before and after mechanical activation. The results indicate that the isoelectric point of raw talc (IEP) was at pH 5.4 and that it was negatively charged above pH =5.5 and positively charged at lower pHs. The results for MAT indicated that the IEP was shifted to around pH 3. This behavior may be attributed to milling energy destroying the Mg-OH bonds as indicated by FTIR spectra, and that the excess of Mg and OH<sup>-</sup> ions in the solution leads to a



compression in the electrical double layer (EDL) of the material, which in turn minimized the magnitude of particle surface charge [37, 38].

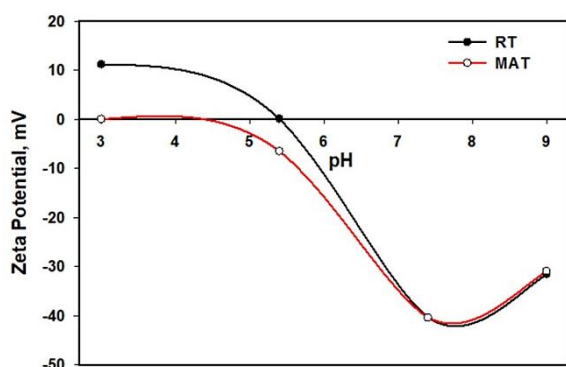


Fig. 6 Zeta potential of RT and MAT.

### 3.5. Surface area analysis

Fig. 7 shows BET adsorption–desorption isotherm for RT and MAT. The pore diameter distribution and specific surface area are shown in Table 3. As displayed in Fig. 6, the characteristic hysteresis loops belong to type B (DeBoer's classification), revealing the mesoporous structure of both RT and MAT.

The BET surface area of MAT was 7.61 m<sup>2</sup>/g, which is three times higher than that of RT (2.48 m<sup>2</sup>/g), and the average pore size was 15.01 nm and 49.29 nm, respectively. As surface area increases and pore size decreases for MAT was probably due to the particles' structure destruction after grinding [39].

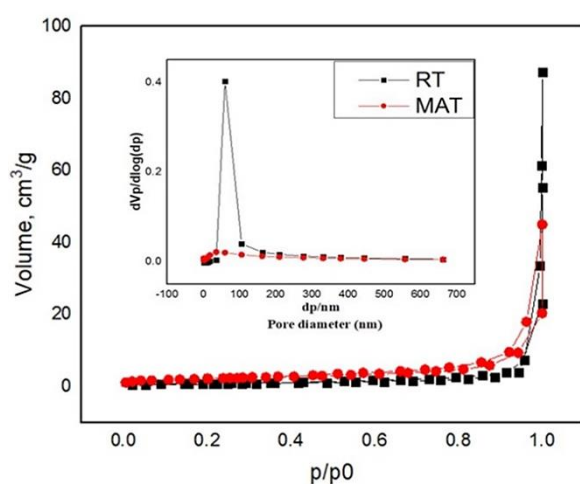


Fig. 7 Adsorption-desorption isotherms and pore size distribution for RT and MAT.

**Table 3.** BET analysis results of RT and MAT from N<sub>2</sub> adsorption isotherms at 77 K.

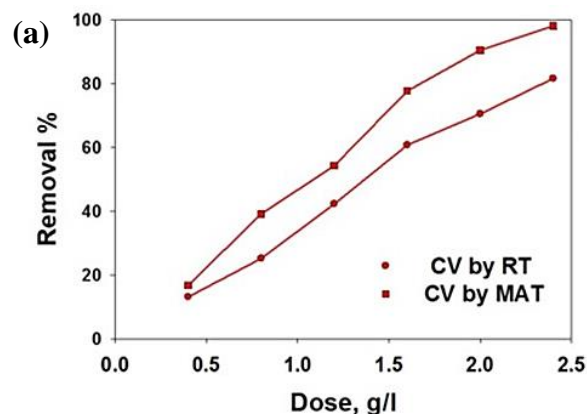
Sample	S <sub>BET</sub> (m <sup>2</sup> /g)	Pore radius (nm)
RT	2.4792	49.295
MAT	7.606	15.01

### 3.6. Dye Removal/Adsorption Study

#### 3.6.1. Effect of dosage

The amount of adsorbent (dose) is a crucial element in the adsorption process since it establishes the adsorbent's suitability for a specific starting dye concentration in aqueous medium. Figures 8a. and 8b. illustrate the effect of different adsorbent doses on both dyes' removal efficiency of CV and AR1 dyes, respectively. Knowing RT was tested first for the adsorption process. Upon increasing the adsorbent dose from 0.4 to 2.4 g/L, the removal efficiency of RT for AR1 and CV increased from 13.1 to 81.7 % and from 10.2 to 64.2 %, respectively. For MAT, the removal efficiency increased from 16.8 to 98.2 % and from 15.6 to 95.7 %, respectively. The increase in adsorption efficiency for MAT relative to RT can be related to the larger surface area and increase in sites of adsorption and contact surface [40].

Overall, MAT showed a higher removal efficiency % than RT which may be attributed to the higher surface area and increased surface active sites as a result of intensive grinding [34]. While lower adsorbent (dose) may reduce the removal efficiency due to insufficient adsorption active sites, excess adsorbent amount may lead to increased costs and uneconomical operation [41]. Thus, the optimal dose used for both RT and MAT was 2.0 g/L to further study AR1 and CV removal from an aqueous solution.



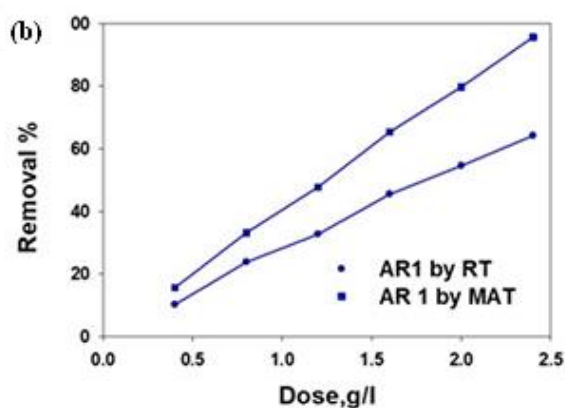


**Fig. 8** (a) Effect of adsorbent concentration on removal % of CV, (b) Effect of adsorbent concentration on removal % of AR1, at  $C_i = 100$  mg/L, pH = 2 for AR 1 and pH=12 for CV, Temp. = 20 °C, and Time = 240 min.

### 3.6.2. Effect of pH

The pH of the solution impacts the dyes' structural stability and, consequently, their color intensity [42]. It also affects the adsorbent zeta potential, as shown before. Figure 9 shows the % of dye removal using the optimal dose of RT and MAT (2 g.L<sup>-1</sup>) for both dyes AR1 and CV over the pH range of 2 - 12. This is because at low pH, more H<sup>+</sup> ions are present that result in the protonation of the adsorbent surface, which in turn enhances the electrostatic interactions between the negatively charged dye molecules (pka= 6.4) and the positively charged adsorbents protonated active sites. This increases the number of dye molecules that are adsorbed [43].

On the other hand, the % removal increased for CV as pH increased for adsorbents RT and MAT. This is because excess H<sup>+</sup> ions present at a low pH competed with the cationic groups of CV (pka = 8.64), resulting in a reduction in the amount of dye adsorbed due to surface repulsion. However, for MAT, the surface charge in acidic regions was close to zero due to the compression of the electrical double layer. This may contribute to the high removal efficiency for the CV (60%) with MAT compared to RT (10%). On the other hand, OH<sup>-</sup> groups are present on the surface of the talc sample the adsorption of cationic dye was increased at high, which is in agreement with other reported data [44]. Overall, the optimal pH for both adsorbents RT and MAT was pH= 2 for AR1 dye and pH = 12 for CV.

### 3.6.3. Effect of contact time

Contact time impact upon the efficiency of removal % and adsorbent capacity is shown in Fig. 10 and 11, respectively, of RT and MAT for AR1 and CV. For RT, an initial slow rate of adsorption for both dyes was observed before reaching equilibrium after 240 min. However, MAT showed a rapid increase in adsorption rate for both dyes within the first ten minutes before reaching equilibrium after 120 minutes. The adsorption of the two dyes on the RT indicates a possible monolayer coverage, while MAT indicates a possible multilayer coverage of dye molecules on the adsorbent surface [42].

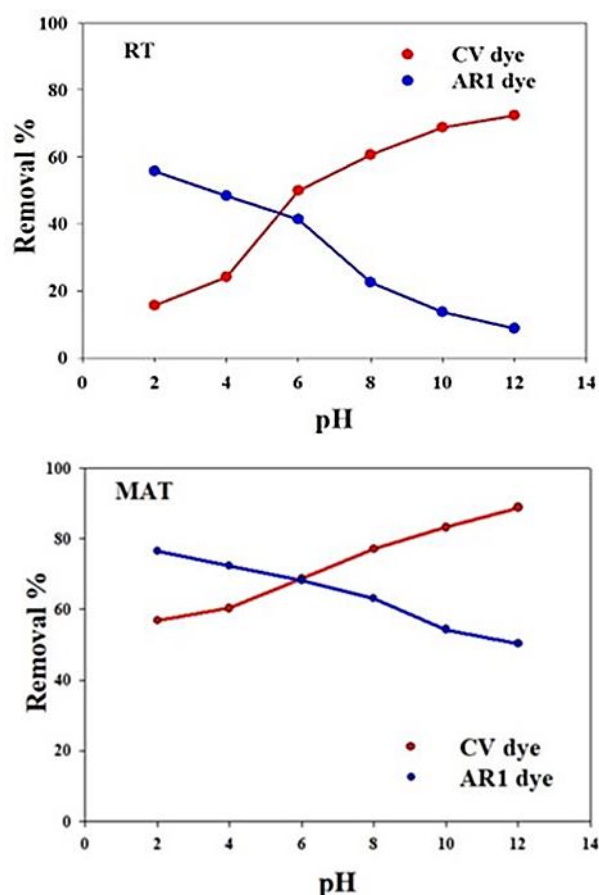


**Fig. 9** Effect of pH on dye removal % using RT and MAT, adsorbent dose = 2 g/L, Temp. =20 °C, Time = 240 min,  $C_i = 100$  mg/L.

### 3.6.4. Effect of initial dye concentration ( $C_i$ )

The effect of the initial concentration of dyes on their adsorption and removal efficiencies by RT and MAT are shown in Figs. 12 and 13. The adsorption capacities of both dyes were increased with the increase in initial dye concentration while the removal efficiency decreased. At low dye concentrations, several accessible sorption sites could hold more dye

molecules. The low removal efficiency at high dye concentrations could result from the adsorbent surface being surrounded by the adsorbate ions and that no more active sites were available for extra dye molecules. The maximum adsorption capacity for CV and AR1 by MAT was 160 mg/g and 130 mg/g, respectively. However, for the RT, it was 80 mg/g and 42 mg/g, respectively. MAT showed high adsorption capacity and high removal efficiency compared to the RT which may be attributed to its high surface, small pore diameter, and multi-charged sites generated because of the rupture of the chemical bond by grinding forces.

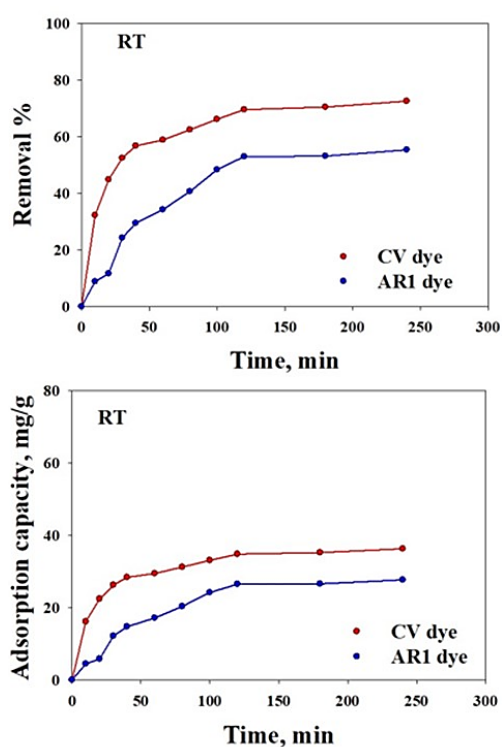


**Fig. 10.** Effect of contact time on the removal efficiency and adsorption capacity of RT, adsorbent dose= 2 g/L, temp. = 20 °C,  $C_i$ = 100 mg/L, pH of cationic dye = 12, and for anionic dye = 2.

### 3.6.5. Effect of temperature

Figure 14 shows that adsorption decreases with an increase in temperature from 20 to 60 °C indicating an exothermic process [45]. This may be because of the increase in dye mobility molecules and their transition from talc's solid to liquid phases [63]. As well, this action could result from weak Van der Waals and dipole forces coupled with low heats of sorption [64, 65].

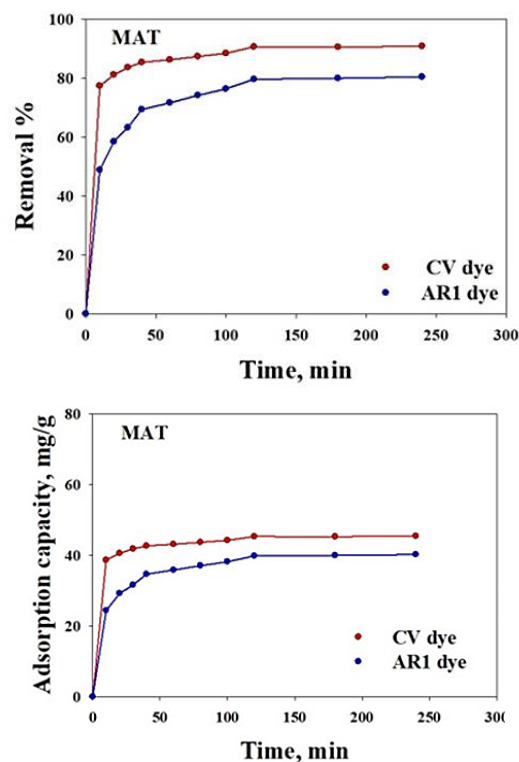


**Fig.11** Effect of time on the removal efficiency and adsorption capacity of MAT, adsorbent dose= 2 g/L, temp. = 20 °C,  $C_i$ = 100 mg/L, pH of cationic dye = 12, and for anionic dye = 2

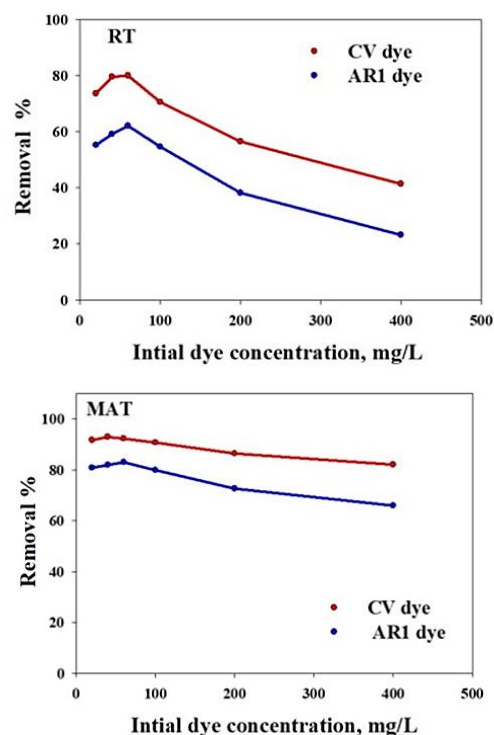


**Fig. 12.** Relation between Initial conc. and Removal % of both RT and MAT, at adsorbent dose = 2 g/l, Temp. = 20 °C, Time = 240 min.

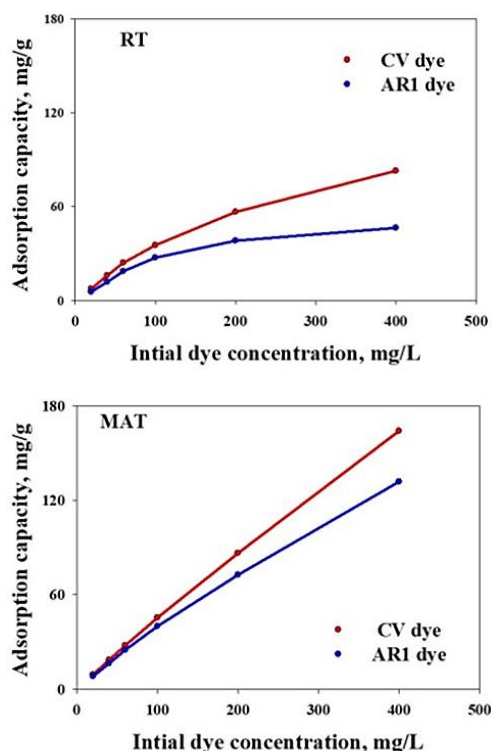


**Fig. 13** Relation between Initial conc. and adsorption capacity of both RT and MAT, at adsorbent dose = 2 g/l, Temp. = 20 °C, Time = 240 min.

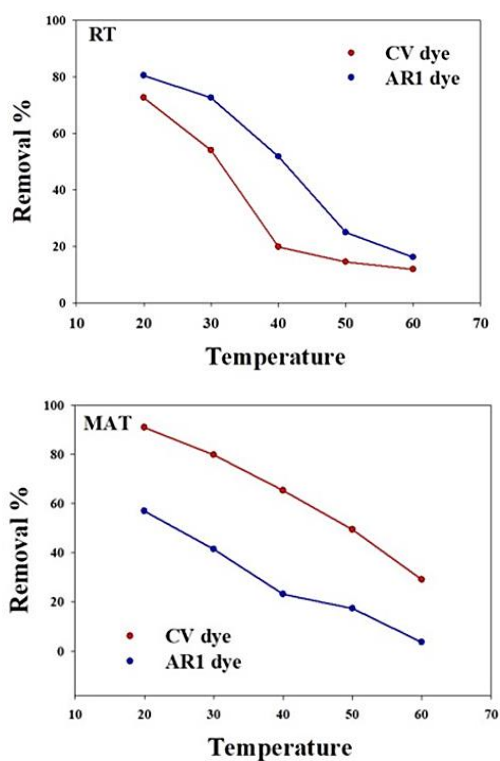


**Fig.14** Effect of temperature on the removal % of dyes, at adsorbent = 2 g/L, pH = 2 for AR1 dye, pH=12 for CV dye, Time =240,  $C_i$ = 100 mg/L.

### 3.6.6. Kinetic studies

To understand the mechanism behind the adsorption process, the adsorption rate was determined via different kinetic models [45]. The pseudo-first-order and pseudo-second-order are common models based on solid capacity and solid phase sorption [46,47]. The intra-particle diffusion model was implemented to calculate the rate of the controlling stage, which is mostly reliant upon pore size or external diffusion [48].

The pseudo-first-order rate is given by equation (3):

$$\ln q_e - q_t = \ln q_e - k_1 t \quad (3)$$

It illustrates the relationship between  $q_t$  (mg/g), adsorbed amount per unit mass at time  $t$  (min), and the  $q_e$ (mg/g), adsorbed amount per unit mass at equilibrium, with  $k_1$  ( $\text{min}^{-1}$ ) being the first order rate coefficient. The displayed plots in Fig. 15 show the data fitting to the pseudo-first-order Lagergren model as the  $q_e$  and  $k_1$  calculated are provided in Table 4.

While the pseudo-second-order reaction rate is given by equation (4):

$$\frac{t}{q_t} = \frac{1}{k_2 q_e^2} - \frac{t}{q_e} \quad (4)$$

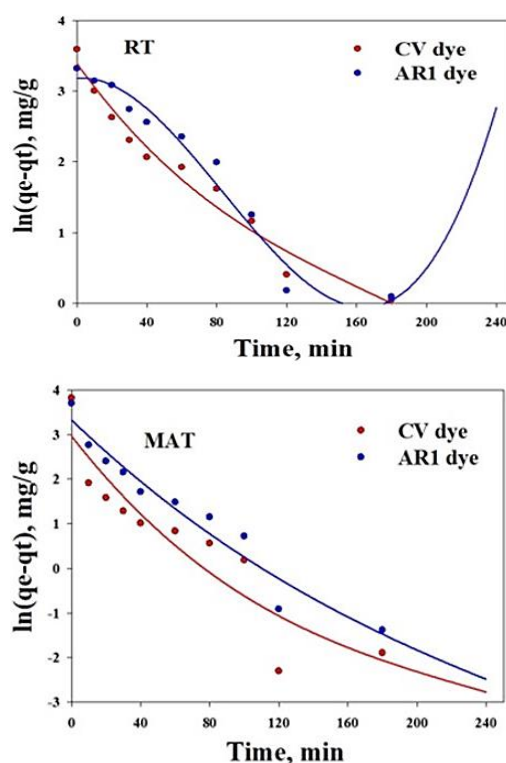


**Fig. 15** Pseudo-first-order kinetic plots  $\ln (q_e - q_t)$  vs time for the adsorption of CV and AR1 on RT and MAT.



where  $q_t$  (mg/g) refers to adsorption capacity at time  $t$ ,  $q_e$  (mg/g) refers to adsorption capacity at equilibrium, and  $k_2$  ( $\text{g}\cdot\text{mg}^{-1}\cdot\text{min}^{-1}$ ) refers to the second-order rate coefficient. The plot in Figure 16 shows the fit of the data to the pseudo-second-order model, and the  $q_e$  and  $k_2$  calculated are provided in Table 4.

The intra-particle diffusion model is an empirical formula (5) that is associated with the adsorbed quantity and  $t^{0.5}$  rather than  $t$  [49].

$$q_t = k_i t^{0.5} + I \quad (5)$$

Where  $q_t$  refers to the adsorption capacity (mg/g) at  $t$  time,  $k_i$  refers to the intra-particle-diffusion constant ( $\text{mg}/\text{g}\cdot\text{min}^{0.5}$ ), and  $I$  indicate the intercept (mg/g), which shows the influence of boundary layer thickness [50, 51]. The plot  $q_t$  versus  $t^{0.5}$  is shown in Figure 17 for the adsorption of AR1 and CV dyes onto RT and MAT. From these figures, it was observed that all lines did not go through the origin, except for anionic dye adsorption on RT. From Table 4, the intra-particle data reveal that diffusion is not the only dominant mechanism as it proceeds as a second-order process but the particle/pore diffusion makes a significant contribution to the adsorption process [42].

According to  $R^2$  in Table 4, the pseudo-second-order model was the most proper model to describe the adsorption kinetics of RT and MAT of CV and MAT by AR1, while the intra-particle diffusion model was the best fit to describe the adsorption kinetics of RT by AR1 dye. This may be attributed to the crystalline structure of raw talc as indicated by the pores size and XRD analysis.

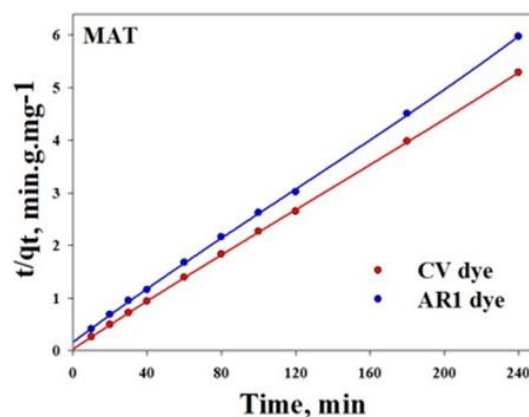
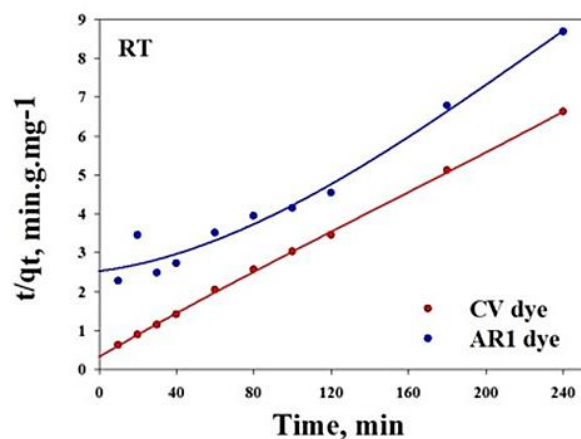


Fig. 16 Pseudo-second-order kinetic plots  $t/qt$  vs time for the adsorption of CV and AR1 on RT and MAT.

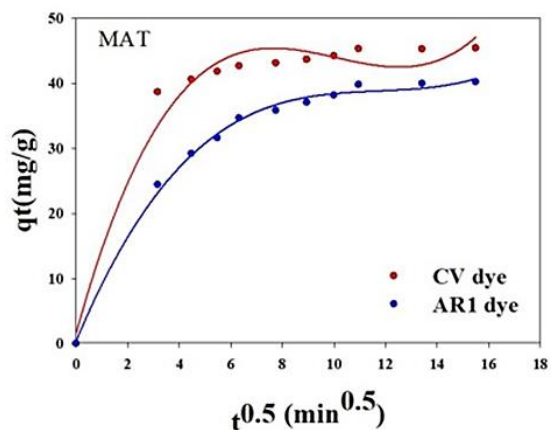
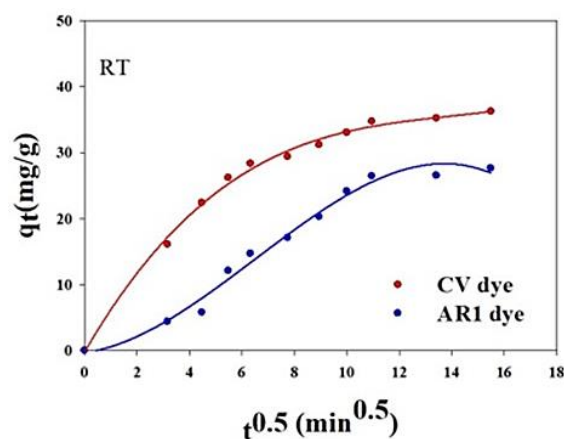


Fig. 17. Model for intra-particle diffusion plots  $q_t$  against  $t^{0.5}$  for the adsorption of CV and AR1 on RT and MAT.

**Table 4.** Calculated parameters from Kinetic study for the removal of AR1 and CV dyes onto RT and MAT adsorbents.

Parameter	(CV)		(AR1)	
	RT	MAT	RT	MAT
<b>The pseudo-first-order equation</b>				
R <sup>2</sup>	0.9699	0.8544	0.9707	0.9488
K <sub>1</sub>	-0.0345	-0.0497	0.0024	-0.0371
Calculated q <sub>e</sub>	29.69	19.34	24.05	27.73
Experimental q <sub>e</sub>	36.2	45.4	27.65	40.2
<b>The pseudo-second-order equation</b>				
R <sup>2</sup>	0.9995	0.9999	0.9727	0.9998
K <sub>2</sub>	2.57 × 10 <sup>-3</sup>	19.3 × 10 <sup>-3</sup>	1.619 × 10 <sup>-5</sup>	4.27 × 10 <sup>-3</sup>
Calculated q <sub>e</sub>	34.6	42.7	156.25	38.0
Experimental q <sub>e</sub>	36.25	45.4	27.65	40.2
<b>The Intra-particle diffusion model</b>				
R <sup>2</sup>	0.9956	0.9684	0.9858	0.9957
I	-0.1849	1.6346	-0.2915	0.4297
K <sub>i</sub>	6.8395	14.3783	0.5356	9.4820

### 3.6.7. Adsorption isotherms

Adsorption isotherm models help to understand the nature of interactions between adsorbate and adsorbents. In this study, the equilibrium adsorption data was investigated by applying the linear representations of the Freundlich, Langmuir, and Temkin isotherm models. The Freundlich isotherm model, defined by equation (6) [25], is particularly noteworthy for its ability to characterize adsorption on heterogeneous surfaces, without being constrained to monolayer formation.

$$\ln q_e = \ln K_F + 1/n \ln C_e \quad (6)$$

where  $C_e$  (mg/l),  $q_e$  (mg/g),  $K_F$ , and  $1/n$  represent the equilibrium dye concentration in solution, the adsorption capacity, the Freundlich constant, and the heterogeneity factor, respectively. The plots of  $\ln q_t$  vs.  $\ln C_f$ , Fig. 18, enable the determination of  $K_F$  and  $1/n$  isotherm constants from the intercept and slope, respectively. The Langmuir isotherm model postulates a rapid decrease in intermolecular forces as distance increases, which leads to the formation of a monolayer coverage of the adsorbate at specific uniform sites on the external surface of the adsorbent, often associated with chemisorption. Equilibrium data for adsorption is

then assessed using the linear representation of the Langmuir isotherm model, as expressed by equation (7) in Figure 19 [52].

$$\frac{C_e}{q_e} = \frac{C_e}{q_{max}} + \frac{1}{b \cdot q_{max}}$$

Where  $C_e$  (mg/l) is the equilibrium dye concentration in solution,  $q_e$  (mg/g) is the adsorption capacity,  $b$  (l/g) is the Langmuir constants, and  $q_{max}$  (mg/g) is the maximum adsorption capacity. The Langmuir separation factor,  $R_L$ , is given by equation (8) [53].

$$R_L = 1 / (1 + bC_i) \quad (8)$$

Where  $b$  refers to the Langmuir constant and  $C_i$  represents the initial dye concentration. The calculated  $R_L$  values indicate the nature of isotherm as  $R_L > 1$ , unfavorable adsorption process,  $R_L = 1$ , linear adsorption process,  $R_L = 0$ , Irreversible adsorption process (strong adsorption), and  $0 < R_L < 1$  signifies favorable adsorption process (normal adsorption). The  $R_L$  values for different initial dye concentrations (AR1 and CV) were between 0 and 1 indicating a favorable adsorption [53, 54].

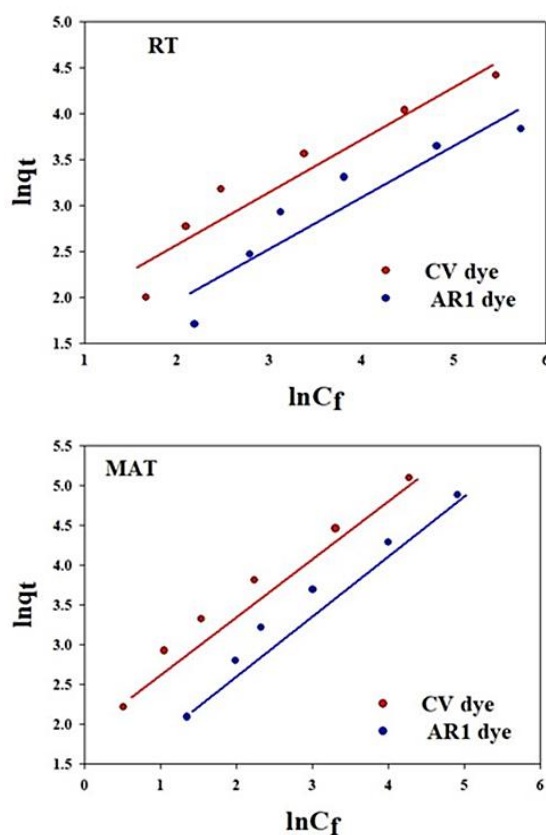


**Fig. 18.** Freundlich adsorption isotherm plots  $\ln q_t$  vs.  $\ln C_f$  for the adsorption of CV and AR1 on RT and MAT.

The Isotherm of Temkin is distinguished by a uniform binding distribution energy and describes the interaction between the adsorbate and the adsorbent [40]. Temkin isotherm has generally been represented by the following equation (9) [55, 56]:

$$q_e = B \ln A_T + B \ln C_e \quad (9)$$

where:  $B = \frac{RT}{b}$  is the heat of sorption constant (J/mol),  $b$  (intercept) = Temkin isotherm constant,  $A_T$  (slope) = isotherm equilibrium binding constant related to Temkin (L/g) obtained from the plot of  $q_t$  against  $\ln C_f$ ,  $R$  is the universal gas constant (8.314 J/mol/K),  $T$  is the temperature at 293 K [57, 58]. The Temkin isotherm parameters were determined from the plot of ( $q_t$ ) versus  $\ln(C_f)$  Fig. 20, and the Temkin isotherm constants for CV and AR1 adsorption onto MAT and RT are presented in Table 5 [59]. According to Temkin's isotherm, adsorption is defined by an equal binding energy distribution up to a maximum binding energy, and adsorption heat steadily decreases as the adsorbate molecules cover the adsorbent surface [60].

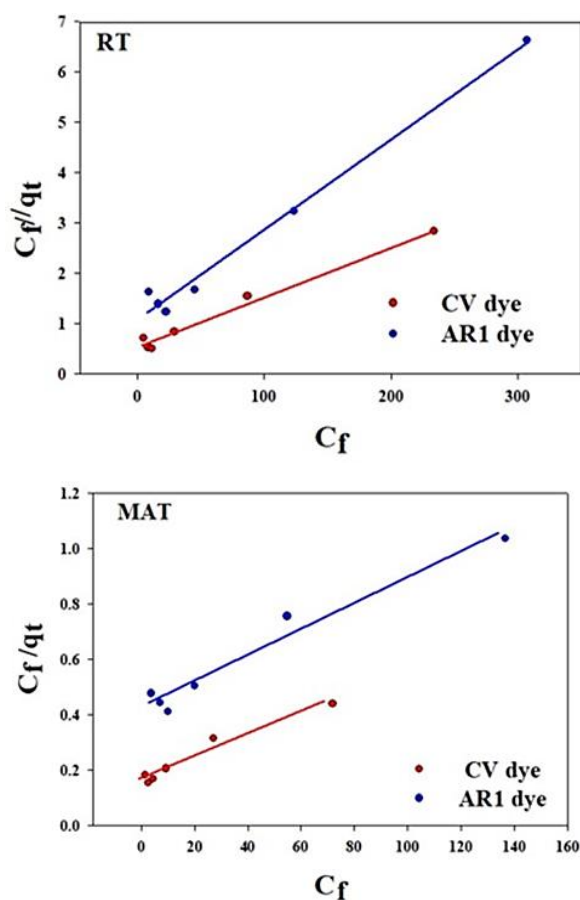


**Fig. 19** Langmuir isotherm plots  $C_f/q_t$  vs  $C_f$  for the adsorption of CV and AR1 on RT and MAT.

From Table 5, Freundlich isotherm may be used to describe the adsorption of AR1 on MAT, which is a highly heterogeneous process and occurs mainly by opposite charge attraction (physisorption) [61]. Temkin isotherm is relatively higher than those obtained for the Freundlich and Langmuir isotherms for CV and AR1 adsorption on RT, so the Temkin isotherm can be used to describe the adsorption of these dyes on RT [48].

According to the values of  $B = (0.006, 0.009 \text{ kcal/mol})$  for CV by RT and MAT, respectively, and  $(0.003, 0.008 \text{ kcal/mol})$  for AR1 by RT and MAT, respectively, which is less than 1 kcal/mol that physical adsorption occurs [57]. The positive values of  $B$  indicate that the adsorption is exothermic at RT and MAT by both CV and AR1 [62].

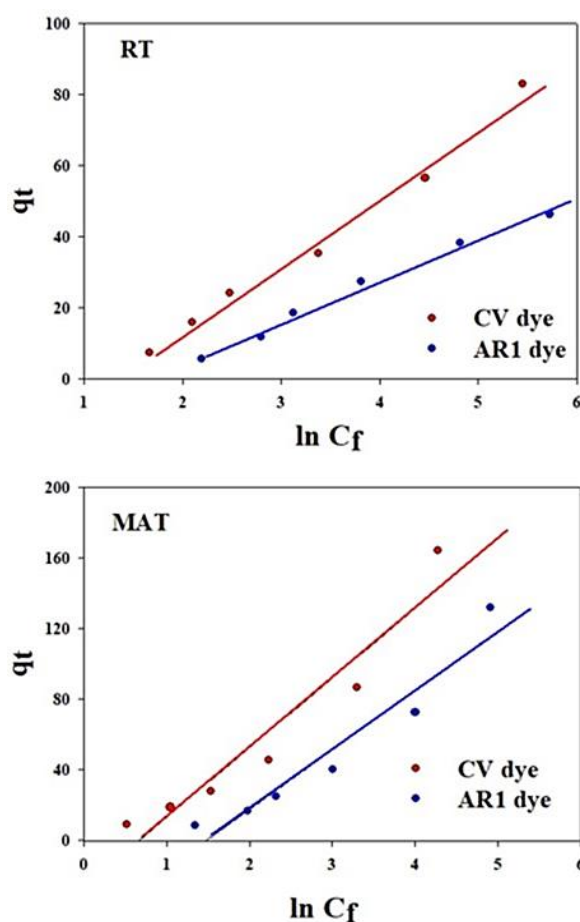


**Fig. 20** Temkin isotherm plots  $q_t$  vs  $\ln C_f$  for the adsorption of CV and AR1 on RT and MAT.

**Table 5** Calculated parameters from isotherm study for AR1 and CV dyes removal by RT and MAT ( $t = 240$  min and  $m = 2$  g) and values of the correlation coefficient  $R^2$

Item	(CV)		(AR1)	
	RT	MAT	RT	MAT
<b>Freundlich Isotherm parameters</b>				
$R^2$	0.9145	0.9819	0.8738	0.9789
$n$	1.75	1.373	1.78	1.329
$K_F$	4.3340	7.93	2.414	3.63
<b>Langmuir Isotherm parameters</b>				
$R^2$	0.9824	0.9548	0.9874	0.9611
$q_{\max}(\text{Cal.})$	100	250	55.9	212.8
$q_{\max}(\text{Exp.})$	82.9	164	46.4	131.8
$b$	0.01902	0.024	0.01695	0.011
<b>Temkin isotherm</b>				
$R^2$	0.9877	0.9215	0.9904	0.9343
$B$ (J/mol)	19.08	39.4	11.8	33.7
$A_T$ (L/g)	0.2686	0.5144	0.1916	0.2277

### 3.6.8. Thermodynamic studies

Evaluation of the sorption process's spontaneity was calculated using the  $K_c$  vs.  $1/T$  graphs, using the following equations (10) and (11):

$$\ln K_c = \frac{\Delta S^\circ}{R} - \frac{\Delta H^\circ}{RT} \quad (10)$$

$$\Delta G^\circ = -RT \ln K_c \quad (11)$$

where  $K_c$  ( $= q_e/C_e$ ),  $R$ , and  $T$  represent the distribution coefficient, the universal gas constant ( $8.314 \text{ J K}^{-1} \text{ mol}^{-1}$ ), and the temperature in kelvin (K), respectively. However, enthalpy ( $\Delta H^\circ$ ), entropy ( $\Delta S^\circ$ ), and Gibbs's free energy ( $\Delta G^\circ$ ).  $K_c$  is a constant for a specific dye concentration and serves as the basis for thermodynamic calculations [44]. RT and MAT values of standard enthalpy ( $\Delta H^\circ$ ) for both dyes were negative indicating exothermic adsorption.  $\Delta H^\circ$  ( $> 40 \text{ kJ/mol}$ ) referred that the process is chemically controlled. The negative values of ( $\Delta S^\circ$ ) for RT and MAT for both CV and AR1 dyes indicate that during the process of adsorption at the solid/liquid interface, a reduction in randomness occurs and it is not favorable at higher temperatures. The Gibbs free energy change values ( $\Delta G^\circ$ ) were negative at low temperatures becoming positive at higher temperatures. This indicates that the adsorption is spontaneous at lower temperatures, and becomes non-spontaneous at higher temperatures, making it unfavorable at higher temperatures. Thus, the process is exothermic.

### 4. Suggested adsorption mechanism

The mechanism for CV and AR1 adsorption on the surface of RT and MAT may be explained depending on the composition, charge, and function groupings of their components. Between two layers of silicate ( $\text{SiO}_2$ )

are layers of magnesium hydroxide ( $\text{MgO} \cdot \text{H}_2\text{O}$ ) that make up talc. Because siloxane groups ( $-\text{Si}-\text{O}-\text{Si}-$ ) are present, it possess hydrophobic characteristics on its basal planes.

Due to the presence of hydroxyl groups ( $-\text{SiOH}$  and  $-\text{MgOH}$ ), the edges are hydrophilic [66]. The bond lengths of Si-O and Mg-OH bonds in talc molecules are 1.624 and 2.069 Å, respectively [67]. These bonds are relatively long compared to other bonds in the talc molecules, giving them priority to be broken first by grinding energy forces. FTIR results confirmed that in the MAT spectrum where the Mg-O/Mg-OH bonds (octahedral layer) and Si-O bond (tetrahedral layer) were destroyed after mechanical activation to create positive and negative sites ( $\text{Mg}^+$ ,  $\text{Si}^+$ ,  $\text{O}^-$ ) as shown in Fig. 21,.. Therefore, the adsorption may occur due to the interaction of the electrostatic charges between  $\text{O}^-$  and the positive charge on CV, in addition to the positive charges  $\text{Mg}^+$ ,  $\text{Si}^+$  and sulfonic group on AR1 [68]. The adsorption on RT may occur because of the hydrophobic interaction between siloxanes in the adsorbent (strongly hydrophobic) and the aromatic rings in the structure of both dyes [66]. As well, H-bonding may occur between the groups of amine in the molecules of CV structure, and groups of ( $-\text{OH}$ ) present in the structure of RT.

**Table 6** Calculated parameters from thermodynamics for AR1 and CV removal using RT and MAT.

(CV)						
Temp. °C	RT			MAT		
	$\Delta H^\circ$ KJ. $\text{mol}^{-1}$	$\Delta S^\circ$ $\text{J.k}^{-1}$	$\Delta G^\circ$ $\text{J.k}^{-1}$ . $\text{mol}^{-1}$	$\Delta H^\circ$ KJ. $\text{mol}^{-1}$	$\Delta S^\circ$ $\text{J.k}^{-1}$	$\Delta G^\circ$ $\text{J.k}^{-1}$ . $\text{mol}^{-1}$
20			-2361			-5600
30			-393			-3456
40	-64	-213	3656	-63	-196	-1639
50			4786			66
60			5568			2472
(AR1)						
Temp. °C	RT			MAT		
	$\Delta H^\circ$ KJ. $\text{mol}^{-1}$	$\Delta S^\circ$ $\text{J.k}^{-1}$	$\Delta G^\circ$ $\text{J.k}^{-1}$ . $\text{mol}^{-1}$	$\Delta H^\circ$ KJ. $\text{mol}^{-1}$	$\Delta S^\circ$ $\text{J.k}^{-1}$	$\Delta G^\circ$ $\text{J.k}^{-1}$ . $\text{mol}^{-1}$
20			-3438			-676
30			-2437			875
40	-66	-212	-172	-67	-225	3129
50			2973			4201
60			4578			9101



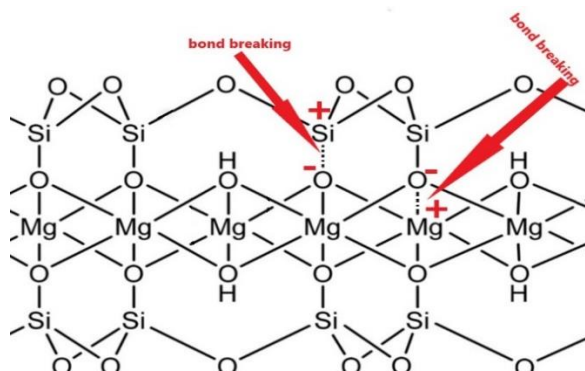


**Fig. 21** Negative and positive sites arise as a result of mechanical activation.

## 5. Conclusions

The present study demonstrates that intensive grinding of the talc sample induces dramatic crystal dislocation, a noticeable shift in its isoelectric point (IEP), an increase in surface area, and significant surface modifications. Modified Activated Talc (MAT) exhibited enhanced efficiency as an adsorbent for Crystal Violet (CV) and AR1 aqueous solution-based dyes. The maximum removal efficiency was achieved at pH 2 for AR1 and pH 12 for CV dyes. Adsorption results indicated that the removal of Reactive Turquoise (RT) for AR1 and CV dyes followed the Temkin isotherm, while MAT for AR1 and CV followed the Freundlich isotherm. The pseudo-second-order kinetic model accurately described the adsorption kinetics of AR1 and CV dyes by MAT and CV dyes by RT. Meanwhile, the intra-particle diffusion model described the adsorption of RT by AR1. Thermodynamic parameters suggest that the process is exothermic and chemically controlled. The negative  $\Delta S^\circ$  indicates a decrease in randomness at the solid/liquid interface during the adsorption process, making it less favorable at higher temperatures. The increase in  $\Delta G^\circ$  with temperature suggests a more favorable adsorption process and increased spontaneity at lower temperatures. Thus, activated talc is considered an effective, low-cost adsorbent for treating wastewater contaminated with textile dyes.

## References

[1] P. Devahi et al., Experimental Investigation on Photo Catalytic Degradation of Textile Effluent Using Hetero Catalyst. *JETIR*, 6 (5), (2019).  
 [2] T. Adane et al., Textile Industry Effluent Treatment Techniques. *Hindawi Journal of Chemistry*, 2021(14), (2021).

[3] H. Halepoto et al., Current status and research trends of textile wastewater treatments—A bibliometric-based study. *Front. Environ. Sci*, 10, (2022).  
 [4] T.C.R. Bertolini et al., Adsorption of Crystal Violet Dye from Aqueous Solution on to Zeolites from Coal Fly and Bottom Ashes. *The Electronic Journal of Chemistry*, 5, (2013).  
 [5] A. Adak et al., Removal of crystal violet dye from wastewater by surfactant-modified alumina. *Separation and Purification Technology*, 44 (2), (2005) 139-144.  
 [6] O .S. Amodu et al., Rapid Adsorption of Crystal Violet onto Magnetic Zeolite Synthesized from Fly Ash and Magnetite Nanoparticles. *Journal of Encapsulation and Adsorption Sciences*, 5, (2015) 191-203.  
 [7] L. Ayed et al., Biodegradation of crystal violet by an isolated *Bacillus* sp. *Annals of Microbiology*, 59, (2009) 267-272.  
 [8] A. Mittal et al., Adsorption of hazardous dye crystal violet from wastewater by waste materials. *Journal of Colloid and Interface Science*, 343(2), (2010) 463-473.  
 [9] T.M.ElMorsi, Synthesis of Nano-Titanium Tannate as an Adsorbent for Crystal Violet Dye, Kinetic and Equilibrium Isotherm Studies. *Journal of Environmental Protection*, 6, (2015) 1454-1471.  
 [10] R. Ahmed et al., Kinetics and Thermodynamics of Acid Red 1 Adsorption on Used Black Tea Leaves from Aqueous Solution, *International Journal of Sciences*, 10(6), (2021).  
 [11] T.Wang et al., Facile fabrication of Fe<sub>3</sub>O<sub>4</sub>/MIL-101(Cr) for effective removal of acid red 1 and orange G from aqueous solution. *Chemical Engineering Journal*, 295, (2016) 403-413.  
 [12] A. Dąbrowski, Adsorption - From theory to practice, *Advances in Colloid and Interface Science*. 93(1-3), (2001) 135-224.  
 [13] S. Khanna, and V. K. Rattan, Removal of acid red 1 from aqueous waste streams using peel of *Cucumis sativus* fruit. *Equilibrium studies. Journal of Chemical Technology and Metallurgy*, 52 (5), (2017) 803-811.  
 [14] C. A. Sophia, and E.C. Lima, Removal of emerging contaminants from the environment by adsorption. *Ecotoxicol, Environ. Saf.*, 150, (2018) 1-17.  
 [15] A.L. Grafia et al., Use of talc as low-cost clarifier for wastewater. *Water Sci Technol*, 69 (3), (2014) 640-6.  
 [16] T. R. C. Oliveira, and M. P. Paiva, Technological Characterization Of Talc Ore From Caçapava Do Sul, Rs-Brazi For Development Of A Process Route. *HOLOS*, 06 (33), (2017) 147-161.  
 [17] T. Ngulube et al., An update on synthetic dyes adsorption onto clay-based minerals: A state-of-art review. *Journal of Environmental Management*, 191, (2017) 35-57.  
 [18] L. Wenlei et al., Adsorptive characteristics of modified talcum powder in removing methylene blue

- from wastewater. *Chemical Speciation and Bioavailability*, 26(3), (2014).
- [19] A.Rahman et al., Adsorption characteristics of clay adsorbents – sepiolite, kaolin and synthetic talc – for removal of Reactive Yellow 138:1. *water and environmental journal*, 29 (3), (2015) 375-382.
- [20] S. Gracis et al., A new classification system for all-ceramic and ceramic-like restorative materials. *Int J Prosthodont*, 28(3), (2015) 227-35.
- [21] N. Behmanesh et al., Role of mechanical activation of precursors in solid state processing of nano-structured mullite phase, *Journal of Alloys and Compounds*, 450(1–2), (2008) 421-425.
- [22] I. Tole et al., Mechanochemical activation of natural clay minerals: an alternative to produce sustainable cementitious binders – a review. *Miner Petrol*, 113, (2019) 449–462.
- [23] E.F. Aglietti, The effect of dry grinding on the structure of talc, *Applied Clay Science*, 9 (2), (1994) 139-147.
- [24] S. M. Palaniandy, Impact of mechanochemical effect on chalcopyrite leaching. *International Journal of Mineral Processing*, 136, (2015) 56-65.
- [25] D. Kirsever et al., Effects of mechanical activation on the structure of talc. *Journal of Ceramic Processing Research*, 16(5), (2015) 544-547.
- [26] K. Y. A. Lin and T. Y. Lin, Degradation of Acid Azo Dyes Using Oxone Activated by Cobalt Titanate Perovskite. *Water, Air, and Soil Pollution*, 229, (2018).
- [27] F. Parisi, Adsorption and Separation of Crystal Violet, Cerium(III) and Lead(II) by Means of a Multi-Step Strategy Based on K10-Montmorillonite, *minerals*,10(5),(2020) 466.
- [28] P. Marzbani et al., Surface Modification of Talc Particles with Phthalimide: Study of Composite Structure and Consequences on Physical, Mechanical, and Optical Properties of Deinked Pulp. *Bioresources*,11(4), (2016) 8720-8738.
- [29] Y.Lu et al., Optimal Synthesis of Environment-Friendly Iron Red Pigment from Natural Nanostructured Clay Minerals. *Nanomaterials (Basel)*, 8(11), (2018).
- [30] H. N. Kim et al., Effects of Ball Size on the Grinding Behavior of Talc Using a High-Energy Ball Mill. *Minerals*, 9(11), (2019) 668.
- [31] L. Boudriche et al., Influence of different dry milling processes on the properties of an attapulgite clay, contribution of inverse gas chromatography. *Powder Technology*, 254, (2014) 352-363.
- [32] L. Liu et al., Study on decomposition kinetics of activated alunite concentrate from copper tailings and leaching behavior of valuable elements, *Cleaner Materials*, 1, (2021) 100008.
- [33] H. Yang et al., Preparation of porous material from talc by mechanochemical treatment and subsequent leaching. *Applied Clay Science*, 31(3–4), (2006) 290-297.
- [34] M. Ossman et al., Peanut shells and talc powder for removal of hexavalent chromium from aqueous solutions. *Bulgarian Chemical Communications*, 46(3), (2014).629–639.
- [35] F. Dellisanti et al., Changes of the main physical and technological properties of talc due to mechanical strain. *Applied Clay Science*, 42 (3–4), (2009) 398-404.
- [36] N.Thi Huong et al., Synthesis Fe<sub>3</sub>O<sub>4</sub>/Talc nanocomposite by coprecipitation-ultrasonication method and advances in hexavalent chromium removal from aqueous solution. *Adsorption Science & Technology*.38(9-10),(2020)483-501.
- [37] Y. Horikawa et al., The effect of electrolyte concentration on the zeta potentials of homoionic montmorillonite and illite. *Colloids and Surfaces*. 32, (1988) 181-195.
- [38] E.E. Saka, and C.GU“ LER, The effects of electrolyte concentration, ion species and pH on the zeta potential and electrokinetic charge density of montmorillonite. *Clay Miner*, 41(4), (2006) 853–861. doi: <https://doi.org/10.1180/0009855064140224>
- [39] A. M. Carvajal et al., Application of the Sips model to the calculation of maximum adsorption capacity and immersion enthalpy of phenol aqueous solutions on activated carbons. *European Journal of Chemistry*, 8(2), (2017) 112-118.
- [40] M.A. Ali et al., Adsorption of crude and waste diesel oil onto agar-carboxymethylcellulose-silver nanocomposite in aqueous media. *Inorganic Chemistry Communications*,133, (2021) 108915.
- [41] H.Xie et al., Effect of the occurrence state of magnesium in talc on the adsorption of Pb(II). *Journal of Alloys and Compounds*, 887, (2021) 161288.
- [42] F. M. S. E. El-Dars et al., Adsorption Kinetics of Bromophenol Blue and Eriochrome Black T using Bentonite Carbon Composite Material. *International Journal Of Scientific and Engineering Research*, 6 (5), (2015) 679.
- [43] U.Kamran et al., Chemically modified sugarcane bagasse-based biocomposites for efficient removal of acid red 1 dye: Kinetics, isotherms, thermodynamics, and desorption studies. *Chemosphere*, 291(2), (2022) 132796.
- [44] Z.Wu et al., Kinetics and thermodynamics of the organic dye adsorption on the mesoporous hybrid xerogel. *Chemical Engineering Journal*, 112 (1–3) (2005) 227-236.
- [45] H .Yuh-Shan., Citation review of Lagergren kinetic rate equation on adsorption reactions. *Scientometrics* 59, (2004) 171–177.

- [46] Y. S. Ho, and G. McKay, The kinetics of sorption of divalent metal ions onto sphagnum moss peat. *Water Research*, 34 (3), (2000) 735-742.
- [47] W. S. Ngah, and M.A.K.M. Hanafiah, Adsorption of copper on rubber (*Hevea brasiliensis*) leaf powder: Kinetic, equilibrium and thermodynamic studies. *Biochemical Engineering Journal*, 39 (3), (2008) 521-530.
- [48] M. M. S. Sanad et al., Graphene-magnetite functionalized diatomite for efficient removal of organochlorine pesticides from aquatic environment. *J. of Environmental Management*, 330, (2023) 117145.
- [49] D.N. Ahmed et al., Waste foundry sand/MgFe-layered double hydroxides composite material for efficient removal of Congo red dye from aqueous solution. *Scientific Reports*, 10 (2042), (2020).
- [50] V.S. Mane et al., Kinetic and equilibrium isotherm studies for the adsorptive removal of Brilliant Green dye from aqueous solution by rice husk ash. *Journal of Environmental Management*, 84 (4), (2007) 390-400.
- [51] B.K. Nandi et al., Adsorption characteristics of brilliant green dye on kaolin. *J Hazard Mater.* 161(1), (2009) 387-95.
- [52] Y. Fu et al., Phenolic hydroxyl functionalized hyper-crosslinked polymers and their efficient adsorption, *Separation and Purification Technology*, 318, (2023) 123817.
- [53] H. Demiral et al., Adsorption of chromium(VI) from aqueous solution by activated carbon derived from olive bagasse and applicability of different adsorption models. *Chemical Engineering Journal*, 144(2), (2008) 188-196.
- [54] R. Ragadhita, and A. B. D. Nandiyanto, How to Calculate Adsorption Isotherms of Particles Using Two-Parameter Monolayer Adsorption Models and Equations. *Indonesian Journal of Science and Technology* 6 (1), (2021) 205-234.
- [55] M.I. Temkin, *The Kinetics of Some Industrial Heterogeneous Catalytic Reactions*, Advances in Catalysis. Academic Press, 28, (1979) 173-291.
- [56] R.R. Krishni et al., Adsorption of methylene blue onto papaya leaves: comparison of linear and nonlinear isotherm analysis. *Desal. Water Treat.* 52(34-36), (2014) 6712-6719.
- [57] M. Erhayem et al., Isotherm, Kinetic and Thermodynamic Studies for the Sorption of Mercury (II) onto Activated Carbon from *Rosmarinus officinalis* Leaves. *American Journal of Analytical Chemistry*, 6(1), (2015).
- [58] U.A. Edet, and A.O. Ifelebuegu, Kinetics, Isotherms, and Thermodynamic Modeling of the Adsorption of Phosphates from Model Wastewater Using Recycled Brick Waste. *Processes*, 8 (6), (2020) 665.
- [59] H. Achraf et al., Removal of Hexavalent Chromium Cr (VI) From an Aqueous Solution by an Industrial Waste from the Steelworks of the Algerian Steel Complex. *Annals of R.S.C.B.*, 25(6), (2021) 5457 – 5474.
- [60] I. Ali et al., Synthesis of composite iron nano adsorbent and removal of ibuprofen drug residue from water. *J. Mol. Liq.* 219, (2016) 858-864.
- [61] S. Hashemian et al., Kinetics and Thermodynamics of Adsorption Methylene Blue onto Tea Waste/CuFe<sub>2</sub>O<sub>4</sub> Composite. *American Journal of Analytical Chemistry*, 4(7A), (2013).
- [62] J. Chang et al., Adsorption of Tetracycline by Shrimp Shell Waste from Aqueous Solutions: Adsorption Isotherm, Kinetics Modeling, and Mechanism. *ACS Omega*, 5, (2020) 3467-3477.
- [63] M. M. Doğan et al., Adsorption kinetics of maxilon yellow 4GL and maxilon red GRL dyes on kaolinite, *Journal of Hazardous Materials*, 165 (1-3), (2009) 1142-1151.
- [64] R. Aravindhana et al., Removal of basic yellow dye from aqueous solution by sorption on green alga *Caulerpa scalpelliformis*. *Journal of Hazardous Materials*, 142(1-2), (2007) 68-76.
- [65] S. Chatterjee et al., Adsorptive removal of congo red, a carcinogenic textile dye by chitosan hydrobeads: Binding mechanism, equilibrium, and kinetics, *Colloids and Surfaces A: Physicochemical and Engineering Aspects*, 299(1-3), (2007) 146-152.
- [66] K. Belkassa et al., Understanding of the mechanism of crystal violet adsorption on modified halloysite: Hydrophobicity, performance, and interaction. *Journal of Hazardous Materials*, 415, (2021) 125656.
- [67] J. H. Rayner, and G. Brown, The Crystal Structure Of Talc. *Clays and Clay Minerals*, 21, (1973) 103-114.
- [68] H. Kandil, and H. Ali, Simultaneous Removal of Cationic Crystal Violet and Anionic Reactive Yellow Dyes using eco-friendly Chitosan Functionalized by Talc and Cloisite 30B. *Journal of Polymers and the Environment*, 31, (2022) 1456-1477.